Thermal diffusivity of periderm from tomatoes of different maturity stages as determined by the concept of the frequency-domain open photoacoustic cell

Daniel Soares Velasco, Mauro Luciano Baesso, Antonio Neto Medina, Dane Danijel Bicanic, Rob Koehorst et al.

Related Articles

A new approach of the doserate measurements in thermoluminescence dating
J. Appl. Phys. 55, 4134 (1984)

Automatic Control Systems, by Richard M. Phelan. Reviewer—
Rev. Sci. Instrum. 49, 276 (1978)

Additional information on J. Appl. Phys.

Journal Homepage: http://jap.aip.org/

Journal Information: http://jap.aip.org/about/about_the_journal

Top downloads: http://jap.aip.org/features/most_downloaded

Information for Authors: http://jap.aip.org/authors

Thermal diffusivity of periderm from tomatoes of different maturity stages as determined by the concept of the frequency-domain open photoacoustic cell

Daniel Soares Velasco,[1] Mauro Luciano Baesso,[1] Antonio Neto Medina,[1] Dane Danijel Bicanic,[2,3] Rob Koehorst,[2] Justin Johan Jozias van der Hooft,[2] and Antonio Carlos Bento[1,a]

[1]*Departamento de Física, Laboratório de Espectroscopia Fotoacústica, Universidade Estadual de Maringá, Av. Colombo 5790, Maringá-Paraná, 87020-900, Brazil*
[2]*Laboratory of Biophysics, Wageningen University, Dreijenlaan 3, 6703 HA Wageningen, The Netherlands*
[3]*Food Quality and Nutrition, Faculty of Food Technology and Biotechnology, University of Zagreb, Pierotijeva 6, HR-1000 Zagreb, Croatia*

The frequency-domain open photoacoustic cell (OPC) approach was used to determine room temperature thermal diffusivity of skins (pericarps) from the raw tomatoes (*Lycopersicon esculetum Mill.*) characterized by the three different stages of ripeness (from immature-green to a mature-red). Periodically interrupted 532 nm laser radiation was used to heat the dry tomato skins, typically 10 mm in diameter and up to 68 μm thick; the modulating frequency f varied from 8 to 150 Hz. Initially, a combined OPC-model that takes into account both, the thermoelastic bending and the effect of thermal diffusion (TD), has been applied. Preliminary results showed that until at least 40 Hz, the effect of TD dominates; above this value the combined model fits the experimental data only poorly. For this reason a less complex OPC-TD approach was applied to all investigated skins instead, which predicts an exponential decrease for the amplitude of measured photoacoustic signal S with increasing f. For a specimen that is simultaneously opaque and thermally thick, S depends on f as $S \sim \exp(-b\ f^{1/2})$ where b is a fitting parameter. The S versus f plot enables one to deduce the numerical value for b which, on its turn allows for the assessment of skin's thermal diffusivity α. Thermal diffusivities obtained for the immature green, orange, and red skins (periderms) are 9.9×10^{-8} m^2 s^{-1}, 7.2×10^{-8} m^2 s^{-1}, and 4.6×10^{-8} m^2 s^{-1}, respectively; the uncertainty was typically 5% of the measured value. © *2011 American Institute of Physics*. [doi:10.1063/1.3530735]

I. INTRODUCTION

Directly from their production, processing, and consumption, food materials are subjected to various physical, mechanical, biological, and thermal processes. As an example, thermal properties of foods are often needed to estimate the thermal load during the storage and are also very important in simulating the heat transfer during thermal treatment of foods.[1] In general, thermal properties of foods can be estimated if their compositions (the fraction of protein, water, solids, fat, carbohydrates, ash, etc.) are known.

Thermal conductivity k (W m^{-1} K^{-1}), thermal diffusivity α (m^2 s^{-1}), and thermal effusivity e (J m^{-2} K^{-1} s$^{-1/2}$) are the three dynamic thermophysical parameters unique to each material. Thermal diffusivity α is related to thermal conductivity k through the relationship $\alpha = k/\rho$ c where ρ is the mass density and c is the specific heat at a constant pressure. The composition, the temperature,[2] the changes in microstructural variables, and specific processing conditions are known to affect the thermal diffusivity. Thermal effusivity (also termed heat penetration coefficient, contact coefficient, or thermal admittance) is defined as $e = (k\ \rho\ c)^{1/2}$

$= \rho$ c $\alpha^{1/2}$. Although effusivity plays a dominant role in transient processes that involve surface cooling or heating this quantity is still relatively unknown.

Various approaches to assess food's thermal diffusivity have been proposed in the course of years. One among the most recent ones is a rapid, reliable, and a user friendly technique that was validated on foods derived from thermally processed tomatoes.[3] The obtained thermal diffusivity proved useful in designing both, the sterilization and pasteurization processes, as well as in controlling the transport, storage and the distribution of foods. Another class of the newly emerging techniques capable of accurate and rapid determination of thermophysical parameters, is that of the photothermal (PT) methods;[4] most frequently used are the photoacoustic spectroscopy (PAS) and several of its variants.[5,6] Strangely enough, the PT methods have remained practically unknown to the food and process engineers so far. Buys *et al.*[7] used the photoacoustic (PA) method to determine thermal diffusivity of periderm originating from potatoes grown in different soils. The feasibility of the PT beam deflection method (also known as a "mirage technique") to determine thermal diffusivity of intact beans characterized by varying hydration levels has been successfully demonstrated by Brown *et al.*;[8] a positive correlation between thermal diffusivity and the water content of beans was found. The extent of the correlation between the thermal diffusivity and the

viscosity of the instant corn dry masa flour (cornmeal dough, actually a corn flour soaked with water and used for cooking Mexican tortillas) was established in the photoacoustic study conducted by Yanez-Limon *et al.*[9] Other interesting PA investigations include some additional properties of biological materials, fungi in tomatoes,[10] emission of ethylene by papaya,[11] and the dependence of thermal diffusivity on the water content in fuel cell membrane such as nafion resin [perfluorosulfonic acid/polytetrafluoroethylene (Teflon®) copolymer].[12]

Another powerful PT method, called PT radiometry (PTR), was used to directly assess thermal effusivity of several raw agricultural commodities.[13] Furthermore, optothermal emission radiometry (OTTER), a variant of PTR, was applied to determine, in a nondestructive and rapid fashion, the hydration level as well as the depth dependent hydration profiles in intact tomato fruits of various cultivars.[14] The most widely used method to determine thermal diffusivity is the one that relies on the PA effect. In a conventional experimental PA arrangement the sample, enclosed in an airtight chamber (PA cell), is exposed to a periodically chopped light beam. It was shown that the magnitude of the PA signal depends on the amount of heat generated in the sample (i.e., on the product of the optical absorption coefficient, the incident intensity and the light-into-heat conversion efficiency of the sample), as well as on how does the same heat diffuse through the sample (that is, on the thermal diffusivity α unique to each material). The conventional PA cell is the term reserved for a configuration in which the illumination of the (solid) sample and the generation of acoustic signal (according to Rosencwaig–Gersho theory) occur at one and the same side of the air-tight chamber. On the other hand the term open photoacoustic cell (abbreviated OPC) used in this paper, refers to the geometry in which the PA cell is sealed by a planar sample which itself is being illuminated at its surface located outside the cell (this is the so called rear illumination). In such a case, the generated heat must first pass through a sample of a given thickness prior to being transferred into gas; this is known as an operation in a transmission mode.

The research study described in this paper explores the potential of OPC for determination of thermal diffusivity of isolated skins from raw tomatoes (*Lycopersicon esculentum Mill.*) characterized by three different stages of maturity (ripeness). Tomato, one of the most popular vegetable crops grown worldwide, is rich in lycopene (most of this pigment is found in tomato skin), a phytonutrient that gives tomato its intense red color and acts at the same time as a powerful antioxidant. Various studies have established that the concentration of lycopene in tomato depends on the cultivar and the fruit maturity.[15–17]

Originally, it was assumed that the OPC signal is due to the contributions of the two effects: that of thermoelastic (TE) bending and the thermal diffusion (TD); therefore experimental data was fitted by the appropriate equation developed for a combined OPC model. At a later stage, a less complicated OPC model (it includes only the contribution of TD which is characterized by an exponential decay) was exploited.
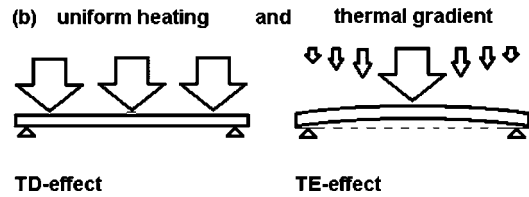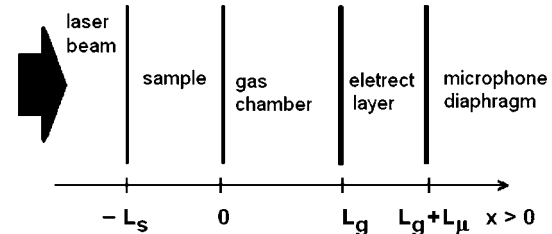

FIG. 1. (a) The generation of the photoaocoustic signal for a rear side illumination geometry and (b) two generation mechanisms (TD and TE bending) for the generation of the thermal piston and mechanic signals.

II. THE OPC THEORY IN THE CASE OF A COMBINED TD AND TE BENDING

A. OPC model in the case of TE bending

The operational principle of OPC is shown in Fig. 1(a). For a periodically heated slab there exist, in general, two distinct mechanisms for the generation of the OPC signal [see Fig. 1(b)]. The first is due to the contribution associated with the process of TD (see scheme left) while the other one is due to the induced TE bending (vibration) as shown in the scheme right. The latter is likely to dominate the OPC signal at high modulation frequencies.[18,19]

The TE bending is a mechanical effect that takes place mainly in the presence of the thermal gradient normal to the surface of the sample. The evidence for this effect was found by several authors; the most commonly used model is that described by Rousset *et al.*[20] These authors solved the TE equations to calculate the displacement of a point at the surface as a function of the thickness (i.e., longitudinal displacement) as well as a function of its diameter (this is sample's radial displacement). McDonald and Wetzel[18] have shown that in the case of a thin, flat slab exposed to a rear illumination, the photoacoustic pressure P_T is due to a combination of the TD (P_{TD}) and the TE effect (P_{TE}). The complete solution for the photoacoustic pressure $P_T = [P_{TD} + P_{TE}]$ is as follows:

$$P_T = \left\{ \left(\frac{C_1}{\sigma_s \sigma_g} \right) \left(\frac{1}{\sinh(\sigma_s L_s)} \right) + \left(\frac{C_2}{\sigma_s^2 \sigma_g} \right) \right.$$
$$\left. \times \left(\frac{\cosh(\sigma_s L_s) - \frac{\sigma_s L_s}{2} \sinh(\sigma_s L_s) - 1}{\sinh(\sigma_s L_s)} \right) \right\} \exp(j\omega t). \quad (1)$$

In the Eq. (1) $\sigma_i(\omega) = (1+j)/\mu_i(\omega)$ the thermal wave vector [subscripts i refer to a gas (g) and sample (s), and j is the complex unity]. TD coefficient defined as $\mu(\omega) = (2\alpha/\omega)^{1/2}$, provides the information about the thermal diffusivity α and depends on the angular frequency ω (since $\omega = 2\pi f$). The
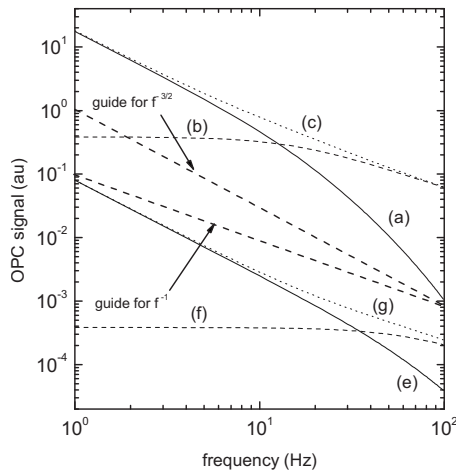
FIG. 2. Simulation for a combined model that incorporates the TD and the TE bending. The characteristic parameters are as follows: L=50 μm, α_1 =10.0×10^{-8} m^2 s^{-1}, C$_1$=3.2×10^9 atm m^{-2}, and C$_2$=1.0×10^4 atm m^{-3} for curves (a)—TD, (b)—TE and (c)—TD+TE, and L=50 μm, α_2=2.5 ×10^{-8} m^2 s^{-1}, C$_1$=3.2×10^9 atm m^{-2}, and C$_2$=1.0×10^4 atm m^{-3} for curves (e)—TD, (f)—TE, and (g)—TD+TE.

amplitude factors C_1 and C_2 in Eq. (1) are defined as: C_1 =$(\gamma P_0 I_0 \beta_s / T_0 L_g K_s)$ and $C_2 = (3\gamma P_0 I_0 \beta_s R_s^4 \alpha_T / R_c^2 L_s^3 L_g K_s)$ ×$(\alpha_s / \alpha_g)^{1/2}$.

In the above relationship for C_1, γ is the ratio of specific heats for air, P_0 and T_0 are the ambient pressure and the ambient temperature, I_0 and β_s stand for the light intensity and the absorption coefficient per unit length, L_g is the thickness of the air gap, and K_s is sample's thermal conductivity. As to the variables appearing in the expression for C_2 the symbols R_s and R_c are the radii of the sample and of the PA cell, L_s is thickness of the sample, α_T is the thermal expansion coefficient, and α_g, and α_s stand for thermal diffusivities of gas (air) and the sample as already described for C_1. The magnitude of the OPC signal can be calculated from the time independent term of the OPC pressure P_T, or from Eq. (1) as $P_T = [S_T] \exp(j\omega t)$.

Under specific experimental conditions it is possible to separate (split) the two contributions of the PA signal in an OPC cell. In the low frequency region the plot that shows the magnitude of the pressure P_{TD} (the latter is responsible for the OPC signal S_{TD}) versus frequency f approaches P_T while P_{TE} might be important at higher frequencies.[19] Thermal parameters of the sample itself and the focusing conditions will determine which of the two frequency regions will dominate. It has been shown repeatedly that TD dominates the OPC signal in the low frequency region where the characteristic slope of the log-log plot for S_{TD} is proportional to $f^{-3/2}$. On the other hand, at higher modulation frequencies and when a very small spot size of radiation (strongly focused beam) is used to heat the sample, the slope of the log-log plot for the OPC signal S_{TE} becomes proportional to f^{-1}. Figure 2 is the simulation of the OPC signal obtained with a combined (TD+TE) model applied to a single polymeric sample characterized by its thickness L=50 μm and two different thermal diffusivities i.e., α_1=10.0×10^{-8} m^2 s^{-1} and α_2=2.5 ×10^{-8} m^2 s^{-1} (these values are in a range typical for polymers such as those of interest here). The two upper curves in

Figs. 2(a) and 2(b), represent the individual contributions (of either TD or TE) in case of higher thermal diffusivity α_1. Dotted curve in Fig. 2(c) is the summation (TD+TE) obtained with C_1= 3.2×10^9 atm m^{-2} and C_2=1.0 ×10^4 atm m^{-3} as weighting constants. Obviously, there is a region where the amplitude for TD decays rapidly with frequency f while the amplitude of TE increases. In such a case, the slope changes from $f^{-3/2}$ to f^{-1} near f=10 Hz; based on this fact it appears that the TE dominates the OPC signal. For other thermal diffusivity limit (α_2=2.5×10^{-8} m^2 s^{-1}, reader should remember that $\alpha_2 < \alpha_1$) one obtains a similar plot for TD but the slope for the magnitude of the OPC signal against the frequency extends further, as it is shown in Fig. 2(e). This time the change in slopes is observed near 50 Hz and the magnitude for TE becomes dominant above 80 Hz [see Fig. 2(f)]. A dotted curve in Fig. 2(g) was obtained when using a combined model (TE+TD) with the same numerical values for C_1 and C_2. In addition, the same figure displays two dashed curves; one shows the slope ($\sim f^{-3/2}$) characteristic for a "pure" TD-domain while the other one refers to the "pure" TE domain where the slope is proportional to f^{-1}.

Such a combined model can be readily used for fitting of data obtained in OPC thermal diffusivity measurements. On the other hand C_1 and C_2 could be regarded as the weighting parameters when trying to estimate the extent of thermoelasticity. In the experiment, one could apply a flat top commercial microphone with an inlet hole size about 3 mm in diameter, which determines the size and the location at which the sample is being fixed. Alternatively, if a microphone top is not flat, it is necessary manufacture a cap provided with a central hole. Such a cap when placed atop the microphone defines the size of the entrance hole and the diameter of the sample. The ratio of the sample and the cell radius as well as the focusing conditions (either a plane wave or the Gaussian spot) may play a detrimental (very important) role in the slope of the OPC signal versus frequency plot. This on its turn may create a situation in the PA experiment where, unlike what is being expected from the generally adopted RG model, the TE bending dominates above the contribution due to the effect of thermal piston.

In the study described here we fit our experimental data by the equations for a combined OPC–(TD+TE) model as well as for the single OPC-TD model; this in order to find out how does TE affect thermal diffusivity of tomato periderm. The comparison of data obtained by a single OPC-TD and the OPC model that includes the contribution due to the TE bending is treated extensively in Sec. IV.

B. The OPC approach in case of a simple TD

Figure 1(a) shows the experimental arrangement typical for measurement of thermal diffusivity by means of an OPC. The OPC is operated in the configuration which is usually referred to as the "transmission mode geometry." The propagation of the generated heat through the sample obeys the laws governing the transport of the energy from a hotter to a colder surface. The underlying theory is based on the mechanism of TD as well as of the conventional Fourier law for heat transfer. The amount of heat deposited (generated) at the

first (external) surface causes the temperature rise to reach a maximum value at the illuminated spot. Once the OPC cell is acoustically sealed by the sample, the temperature at the opposite (internal) side will be lower than that at the surface. In the "transmission mode" geometry the heat geometry the heat propagates into the OPC cell and the sample (generally in a form of a flat slab) provides a tight acoustic seal. In the OPC design the signal to noise ratio is enhanced due to a fact that the volume of the chamber is minimized.[6]

The oscillating pressure P(f) in the photoacoustic cell can be found by solving differential equations for TD using the boundary conditions for a rear side illumination, geometry of which is shown in Fig. 1(a). When TD is the only effect taking place and the sample is opaque and also thermally thin [this latter implies that sample's thickness L_s is much smaller than the TD length $\mu(f)$ at a given modulation frequency f, i.e., $Re(\sigma_s L_s) \ll 1$], the expression for P(f) in Eq. (1) can be rewritten as:

$$P(f) \approx \frac{\gamma P_0 I_0 \alpha_S \sqrt{\alpha_g}}{(2\pi)^{3/2} L_s T_0 L_g K_S} e^{j(\omega t - 3\pi/4)} \left[\frac{1}{f^{3/2}} \right];$$
$$\text{for } L_s \leq \mu(f). \quad (2)$$

In Eq. (2) γ is a ratio C_p/C_v of heat capacities, L_g represents the thicknesses of the gas layer, P_0 and T_0 are the atmospheric pressure and the room temperature, I_0 is the intensity of incident radiation, while K_s and α_s refer to the thermal conductivity and thermal diffusivity of the sample and gas (α_g), respectively. Thermal diffusion length $\mu(f)$ is a function of frequency f and thermal diffusivity since:

$$\mu(f) \equiv \sqrt{\frac{\alpha_S}{\pi f}}. \quad (3)$$

On the other hand, in the case of an optically opaque (absorption takes place at the surface) and thermally thick [i.e., $Re(\sigma_s L_s) \gg 1$] sample specified by the condition $L_s \geq \mu(f)$, relationship for P(f) decreases exponentially with f according to:[6]

$$P(f) \approx \frac{\gamma P_0 I_0 \sqrt{\alpha_S \alpha_g}}{\pi T_0 L_g K_S} e^{j(\omega t - \pi/2)} \left[\frac{e^{-L_S \sqrt{\pi f/\alpha_S}}}{f} \right];$$
$$\text{for } L_s \geq \mu(f). \quad (4)$$

The amplitude S(f) of the photoacoustic signal, in fact the time independent part of P(f), satisfies the relationship:

$$\|P(f)\| \propto S(f) \approx \left[\frac{e^{-b\sqrt{f}}}{f} \right]. \quad (5)$$

Thermal diffusivity α_s is obtained by fitting for parameter b in Eq. (5) defined as:

$$b \equiv L_S \sqrt{\frac{\pi}{\alpha_S}}. \quad (6)$$

III. MATERIAL AND METHODS

A. Preparation of samples

Whole raw tomatoes (*Lycopersicon esculentum Mill.*) at different stage of ripeness: green ($\sim$27 days), orange
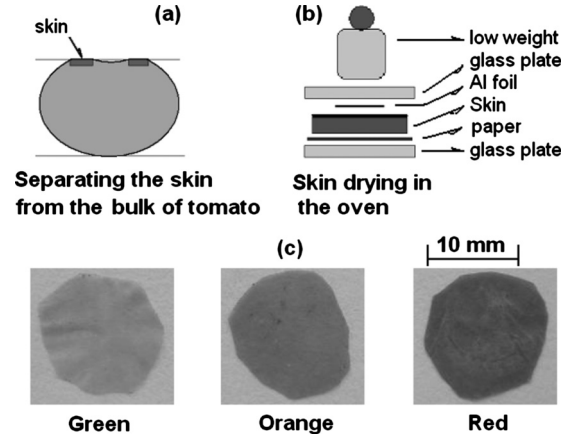

FIG. 3. (a) Separating the skin from the bulk of tomato, (b) drying of skins performed prior to the OPC measurements, and (c) dehydrated skins: green (after 27 days), orange (after 37 days), and red (after 47 days).

($\sim$37 days), and red ($\sim$47 days) were obtained at a local market. Prior to actual thermal diffusivity measurements, skins were separated from the tomato bulk. Initially, an incision (in a form of the letter X) was produced at the location where the tomato fruit was attached to the plant. Tomato was soaked in warm water (60 °C) which caused the skin to loose slightly. Next, the scalpel was used to peel off the skin from the bulk. Because such attempts have met only with a moderate success, upon the separation the skins were rinsed with a cold running water (20 °C) to remove as much as possible bulk residue. Three skin patches (about 1×1 cm^2 each) from each tomato were first mounted between a sheet of paper and an aluminum foil and then placed in an oven maintained at 67 °C for 24 h. Such a procedure helped to remove the skin but at the same time increased the mositure level. This latter is an undesirable because it may alter experimental conditions considerably. In order to overcome this problem a simple procedure was proposed and used to bring the moisture level down to that typical for a tomato prior to soaking in warm water. Dry skins were removed from the oven and left to equilibrate for another 24 h at the room temperature. Figures 3(a) and 3(b) show the sequence of steps followed to remove the skins from raw tomatoes thereby obtaining samples suitable for OPC experiments. The life size images of the skins originating from three different tomatoes are displayed in Fig. 3(c). Overall, thermal diffusivity measurements were conducted on nine different skins, i.e., dry skins of each tomato (green, orange, and deep red) were studied in triplicate.

During the OPC studies on wet skins various problems have been encountered. The first observed undesirable effect was the drying of the skin caused by the modulated incident laser radiation itself. All OPC measurements were performed with the laser light striking the outer, glossy part of the skin. After irradiating tomatoes with the laser light for some time, dark spots on the skins were observed. Such phenomenon, most likely caused by the dehydration of the skin, may affect the steady state conditions of the skin to such extent that the adopted model for thermal diffusivity measurements of a thin solid foil no longer applies. In addition, the OPC data obtained from wet skins showed no evidence for the exponen-
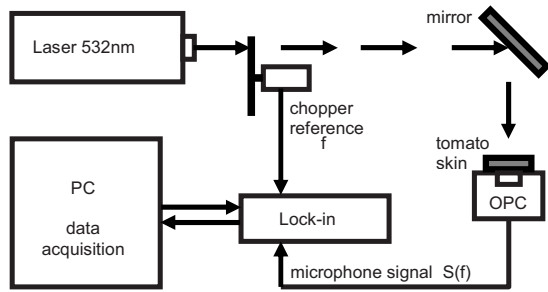
FIG. 4. The experimental set-up for thermal diffusivity measurements by OPC method.

tial decay of the OPC signal; such an observation is contradictory to predictions based on the existing TD model valid for the generation of PA signal in the rear illumination geometry. Therefore one has decided to proceed by performing the measurements only on dry skins and the OPC data thus obtained was used to compute thermal diffusivity.

B. Experimental setup

The experimental set-up used in this OPC study is shown in Fig. 4. The semiconductor c.w. laser (emitted output power 150 mW) was used as the excitation source at 532 nm to generate the OPC signal. The laser beam was mechanically modulated at frequencies between 8 and 150 Hz and the phase and the magnitude of OPC signal recorded with the SR830 Stanford dual-phase vector lock-in amplifier. Thin layer of vacuum grease when spread between the skin sample and the periphery of electret microphone's (Sennheiser, KE-4-211-2) cartridge provided adequate sealing of the OPC chamber. Parameters for our experiment were $R_c = 1.5$ mm, the thickness L_g of the air gap is 1 mm, the diameter of the laser spot is 3.0 mm and the radio of the circumference fixing sample to OPC cell is $R_s = 2.0$ mm.

Thermal diffusivity α_s of a specific skin (periderm) was deduced from a plot featuring the experimentally obtained OPC signal as a function of the modulation frequency. Ideally, a microphone with a flat response over a wide frequency range is preferred in OPC measurements because in such a case there is a direct proportionality between the OPC signal and the pressure. However, this rarely occurs in practice because at the frequencies of a few dozens of hertz the signal to noise ratio begins to deteriorate. Expanding the useful range toward lower frequencies and enhancing of the signal to noise ratio can be achieved but only at the expense of the loss in the linearity of response. The response of the electret microphone used in our experiment was not constant (uniform) across the investigated frequency range. Therefore the procedure was taken [see Figs. 5(a) and 5(b)] to compensate for this effect; the circles represent the microphone response (termed S_{Exp}) obtained from a thin aluminum foil. Obviously, at frequencies below 40 Hz such plot is not a straight line as predicted by Eq. (2). Fitting of data (circles) in a frequency the region exceeding 40 Hz yields a slope of -1.452 ± 0.006. The line shown in the same figure is not a voltage but the numerically generated data (S_{OPC}) obtained when OPC signal depends on frequency with $f^{-1.452}$ throughout the entire (from 8 to 100 Hz) frequency range. This data is in a good
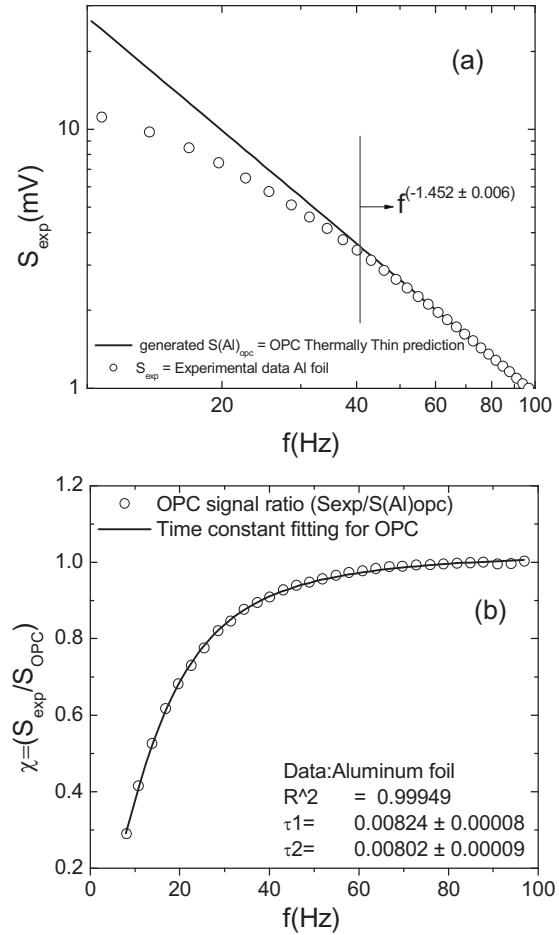

FIG. 5. (a) Typical decay (with $\tau_{avg} \sim 8.0$ to 8.2 ms) of the OPC signal for a thermally thin aluminum foil and (b) fit to the response function of the Sennheiser microphone (type KE-4-211-2) coupled to the OPC.

agreement with that predicted by Eq. (2) for a thermally thin foil. From both data (the circles and the line) in Fig. 5(a) one can obtain the correction factor needed to scaling experimental data collected at the lower modulation frequencies. This latter was achieved by computing the ratio $[S_{Exp}(f)/S_{OPC}(f)]$ shown in Fig. 5(b) (circles). Typically, a continuous line in Fig. 5(b) is the response $\chi(f)$ in a low frequency region ($f < 50$ Hz) for which $\chi(f) \langle 1$ as well as in the frequency region exceeding 50 Hz where this function goes to saturation and $\chi(f) \approx 1$. The required function $S_{Exp}(f) \equiv \chi(f)S_{OPC}(f)$ can be obtained [using the known $\chi(f)$] by using an aluminum foil that simultaneously satisfies conditions imposed on a thermally thin and optically opaque (strong light absorber); in such a case the Eq. (2) becomes $S_{OPC}(f) \approx A \times f^{-B} \approx cte \times f^{-3/2}$, with $cte = (\gamma P_0 I_0 \alpha_s \sqrt{\alpha_g}/(2\pi)^{3/2} L_s T_0 L_g K_s)e^{-3\pi j/4}$ being independent of time or frequency.

The correcting procedure was conducted prior to fitting thermal diffusivity of the skins. The response function that compensates for the non-linear response at frequencies below 50 Hz can be expressed by Eq. (7)

$$\chi(f) \equiv \frac{S_{Exp}(f)}{S_{OPC}(f)} \approx \frac{S(Al)_{measured}}{f^{-3/2}} \approx \frac{2\pi f \tau_1}{\sqrt{[1 + (2\pi f \tau_2)^2]}}. \quad (7)$$

Equation (7) scales the magnitude of the photoacoustic (OPC) signal at low modulation frequencies (thermally thin

TABLE I. Results obtained with a combined (OPC model using fitting parameters C_1, C_2 and α from Eq. (1) predicting the TE bending. The OPC data obtained from Eq. (5) with the fitting parameter b. Both compare data for thermal diffusivity obtained for the dry skins of three tomatoes characterized by a varying maturity stage.

Sample	Thickness (μm)	Fitting with a combined model[a] OPC-(TD+TE), Eq. (1)				Fitting with OPC-TD approach neglecting TE-effect, Eq. (5)	
		C_1 (10^6 atm m^{-2})	C_2 (10^{10} atm m^{-3})	Standard error (10^{-6})	Thermal diffusivity (10^{-8} m^2 s^{-1})	Parameter b (s$^{1/2}$)	Thermal diffusivity (10^{-8} m^2 s^{-1})
Green skin	68 ± 1	7.15	2.57	1.44	$3.86 \pm 2\%$	-0.383 ± 0.019	$9.92 \pm 5\%$
Orange skin	45 ± 1	3.42	6.37	0.13	$2.34 \pm 4\%$	-0.297 ± 0.012	$7.23 \pm 4\%$
Red skin	41 ± 1	0.88	0.39	0.17	$0.77 \pm 5\%$	-0.339 ± 0.010	$4.59 \pm 3\%$

[a]The Levenberg-Marquardt algorithm was used here for the least square fitting procedure.

region). In fitting the transient response of the microphone, τ_1 and τ_2 in Eq. (7) above represent the contributions from electret microphone and from the external pre-amplification circuit,[6] respectively. The solid line in Fig. 5(b) is the best fit to responses ($\tau_1 \cong 8.24$ ms and $\tau_2 \cong 8.02$ ms) of the OPC data obtained from a thermally thin aluminum foil.

IV. RESULTS AND DISCUSSION

A. The calibration of the OPC and fitting for TE effect

The thickness of the tomato skin was measured with a digital micrometer from Mitutoyo having the accuracy of 1 μm. Data in Table I refers to thicknesses measured at the locations where the skins were struck by the laser radiation. Three skins (area approximately 1 cm^2 each) of each tomato have been investigated as quoted above. Figures 6 and 7 show the outcome of the fitting procedure; only one out of the three results obtained with the skin of each tomato is shown. Before the fitting procedure, raw experimental data was divided by $\chi(f)$ [see Eq. (7)] to compute the corrected photoacoustic (OPC) signal. The coordinate axis for the experimental data named S_{corr} and represented by symbols

(data points) shown in Fig. 7(a) was corrected for each sample by calculating the ratio $[S_{Exp}(\text{skin})/\chi(f)]$ upon obtaining $\chi(f)$ with the Al foil used as a test sample. The voltage $S_{Exp}(\text{skin})$ is the signal measured from the tomato skin (periderm).

Figure 6 shows the result of fitting the data for the tomato skins by the combined model that considers the TE bending as well as TD. Due to the fact that both, TE and TD can contribute to a OPC signal in a thin slab, the OPC signal for each of the two mechanisms will, depending on the thermal diffusivity of the sample, exhibit a different slope in the TE or the TD region. The analysis of data obtained with the combined model (Fig. 6) provides the evidence for a dominating effect of TD at frequencies below 50 Hz where the
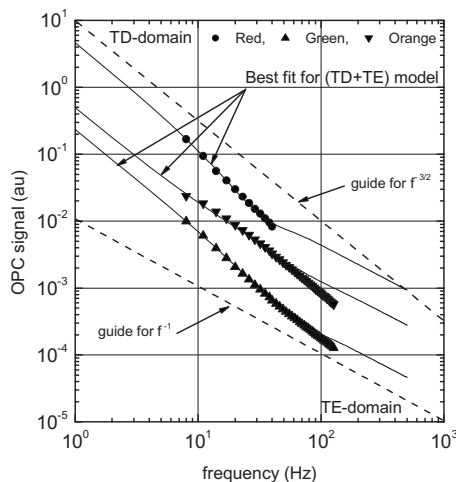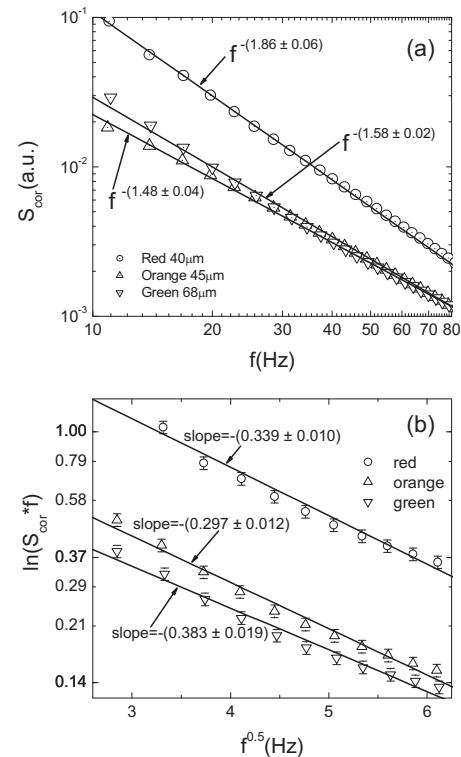

FIG. 6. Log-log analysis of data obtained by a combined model that considers the effect of TE bending. Symbols refer to S_{corr} for periderms of green, orange, and red tomatoes recalculated by using the $\chi(f)$ function. Lines are for the fitting curves obtained by using the Eq. (1). The best fit is found in the low frequency region where TD dominates; the three curve fits exceeded experimental data with the slopes resembling the f^{-1} dependence with f. At frequencies above 50 Hz fitting of data by means of the Eq. (1) indicates a weak TE effect.

FIG. 7. (a) The log-log plot showing the amplitude of the OPC signal vs the modulation frequency f. The decay of the amplitude for the red, orange, and green skins proceeds according to $f^{-1.86}$, $f^{-1.48}$, and $f^{-1.58}$, respectively. Such trend is consistent with that expected for an optically opaque sample in the thermally thick regime. (b). The semilog plot showing the fits to a single exponential function; the corresponding slopes for three tomatoes are $b_{red} = -0.339$, $b_{orange} = -0.297$, and $b_{green} = -0.383$, respectively.

signal decreases in proportion to $f^{-3/2}$. The domain to which the latter slope does apply is shown by a dashed line at the top of the log-log plot in Fig. 6. Up to 50 Hz all experimental data for the skins from green, orange and red tomatoes could be fitted reasonably well with the combined (TD+TE) model described by Eq. (1). On the other hand, a good fit was not observed in a higher frequency region where the TE bending would otherwise dominate the generation of the OPC signal. All three curves display tailoring effects with the slopes tending to f^{-1}.

Fitting the experimental OPC data with the Eq. (1) for a combined model (TD+TE) gives a poor match (significant discrepancy at frequencies above 50 Hz) suggesting a negligible effect of TE bending in this case. The values predicted by this fit go off the experimental data for all analyzed samples. These fits are represented by continuous lines and can be compared to the slope expected for a contribution of a simple TE shown by a dashed line (at the bottom of the frame) which is regarded as indicative for the extent of the TE-domain. This brings one to a conclusion that, unlike what is being expected for a thin slab exposed to a periodic heating, TE bending is not a dominant process and that the TD prevails in the tomato periderms analyzed here.

As to the skin of the tomato, its thermal diffusivity is expected to be very low in comparison with the samples such as metals which definitively do exhibit the bending when heated with a strongly focused radiation (typical a laser beam). In such a case data fitted by Eq. (1) yield thermal diffusivity values ranging from 0.5 to 5.0×10^{-8} m^2 s^{-1} with the error estimated to be less than 10%. In Table I these values are compared to those obtained when fitting data by means of Eq. (5) valid for a simple OPC-TD model.

Rousset and Lepoutre[20] discussed such effect for the case of a flat metal foil (fixed at its edge) characterized by L=0.5 mm, R_c=14 mm, and R_s=16 mm and irradiated by a spot 0.5 mm in diameter. At the modulation frequency of 100 Hz the amplitude associated with the TE bending was 0.5 Å. This was detected by means of the He–Ne probe beam laser propagating parallel to the surface of metal samples such as 304L stainless steel, nickel and zinc. The characteristic frequency f_c defined as $f_c=(\alpha/l_s^2)$ is 15 Hz for 304L stainless steel ($\alpha=3.7 \times 10^{-6}$ m^2 s^{-1}) and 86 Hz for nickel for which $\alpha=21.0 \times 10^{-6}$ m^2 s^{-1}. Such low frequencies are expected because thermal diffusivity of metals is typically hundred times higher than that of a conventional polymer foil exposed to the experimental conditions that favor the occurrence of the TE bending. For 0.050 mm polymer foil thick with α typically on the order of 10 to 20 $\times 10^{-8}$ m^2 s^{-1} one expects f_c to take values between 40 and 80 Hz assuming comparable experimental conditions. Hane and Hattori[21] who have also discussed the phenomenon of thermoelasticity, performed experiments to investigate the effect of the bending on the platelike specimens. In that experiment a 80 μm thick plate of borosilicate glass was fixed to a circular flange with a free diameter of 12 mm. In order to achieve uniform absorption of the laser radiation a 30 nm thick layer of chromium was sputtered on the front surface of the glass plate. A pump diode laser beam (0.5 mm in diameter) strikes the surface of the chromium layer and the sub-sequent heating produces TE bending. The latter is detected by a He-Ne probe beam laser that traverses the heated region parallel to the surface. For a glass plate with $\alpha=77.0 \times 10^{-8}$ m^2 s^{-1}, the characteristic frequency is about 90 Hz. The magnitude of the signal due to the bending is of relevance only when f exceeds f_c, i.e., the region where the slope is proportional to f^{-1}.

B. Thermal diffusivity measurement using OPC TD

The plot of log S_{corr} versus the log of f (circles and triangles pointing up and down) shown in Fig. 7(a) was fitted by a straight line. The slope of the line is larger than -1 revealing that TD is a major mechanism that governs the generation of the signal. Numerical values of slopes vary between -1.48 and -1.86 suggesting a strong signal attenuation due to an exponential decay predicted by Eqs. (4) and (5) for an opaque and thermally thick sample. After convincing evidence for the correctness of the preliminary test has been collected, one has proceeded with the fitting procedure [Eq. (5)]. The corrected amplitudes were then used to construct the semi-log plot shown in Fig. 7(b). From the slope of the straight line one first computes the fitting parameter b and then calculates [Eq. (6)] thermal diffusivity of the skin provided however its thickness is accurately known. The b values for three skins were -0.339 (red), -0.297 (orange), and -0.383 (immature-green). Typical scatter observed for b is about 4.9% for the red skin, 4.0% for the orange skin and 2.9% for the green skin. The extent of the scatter in the b values (when skins were taken from one and the same tomato) on thermal diffusivity calculated from Eq. (6) is between 3% and 5%.

Thermal diffusivity α of dry tomato skins determined by OPC method (Table I) varies between 5.0×10^{-8} and 10.0×10^{-8} m^2 s^{-1}; this range is typical for foods. Most of thermophysical properties of fruits and vegetables reported in the literature refer to a bulk rather than to the skin. For example, thermal diffusivities of apricot jam, mushroom sauce, olive pate, and tomato juice range between 12.0×10^{-8} and 21.0×10^{-8} m^2 s^{-1}.[3] For cassava, plantain and yam the values of α are between 6.0 and 17.0×10^{-8} m^2 s^{-1} when the relative humidity changes from 18% to about 79%.[22] Gordon and Thorne[23] reported thermal diffusivity ranging from 9.0 to 32.0×10^{-8} m^2 s^{-1} for various foods. As to tropical fruit (examples are grapefruit and orange) and vegetables (potato, carrot, yucca, and sugar beet) thermal diffusivity ranges between 13.5×10^{-8} and 17.6×10^{-8} m^2 s^{-1} when moisture content is as high as 90%.[24] The pulp of banana has somewhat higher thermal diffusivity (19.0 to 29.0×10^{-8} m^2 s^{-1}),[25] while α for tomato puree is 15.0×10^{-8} m^2 s^{-1}[26] as compared to 13.0×10^{-8} and 14.0×10^{-8} m^2 s^{-1} reported for the apple juice[27] and peeled potatoes.[28]

Thermal diffusivity of dry tomato skins obtained in this study represents original data for this kind of samples and is within the range of values found for other foods. Another investigation concerned with tomato ripening is that of Bargel and Neinhuis.[29] They measured the elastic modulus of the tomato skin and showed that the elastic modulus in-
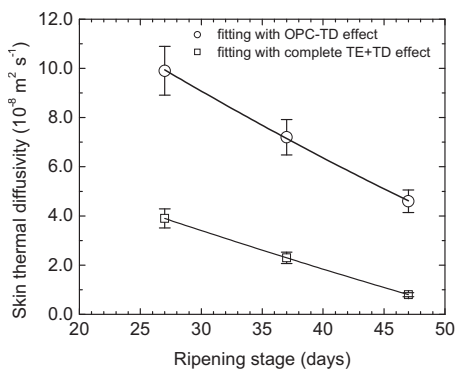
FIG. 8. The correlation between thermal diffusivity of dry tomato skins and their corresponding stage of ripening. The error bars refer to the three independent measurements of skin. Thermal diffusivity α was calculated by means Eq. (6) after fitting the experimental data to Eq. (5) in order to have the best fit for parameter b. Three patches of the skin of each color have been measured and plots refer to both model used for fitting. The combined OPC model Eq. (1) produces lower value for thermal diffusivity.

creases from 100 to 300 MPa in proportion with the stage of ripening. Higher tensile stiffness was ascribed to the role that walls of the epidermal cells play in contributing to the mechanical properties of the fruit's skin.[30] It is the exocarp which contains the cellulose network that reinforces the polymeric structure enhancing at the same time the mechanical stability of the cuticle; similar arguments are likely to apply to the thermal properties as well.

Thermal diffusivity of dry tomato skins decreases monotonously (Fig. 8) reflecting possibly the changes induced in the exocarp of tomato as a fruit matures from a green to a red stage. The OPC-TD model provides better fit to experimental data. Figure 8 also shows the same tendency when data is fitted by the combined TD+TE model; the reader should observe similar slopes for the two sets of data in this figure. The error bars in Fig. 8 refer to a series of three independent measurements performed on the skins of each tomato using the fitted b values. Thermal diffusivity of a skin originating from a red tomato is approximately a half of that measured at the initial ripening stage (green tomato). Microstructures as well as the cross-linked chains in polymers play an important role in the heat diffusion through the polymers. Due to a reduced elasticity of the membrane, the process of ripening is likely to correlate with an enhanced hydrophilic character of the cuticular layer. Yet, fluid and pasty specimens may hold larger quantities of water and consequently their thermal diffusivities are expected to approach that of water. As such, values for thermal diffusivity (which determines how quickly certain product heats or cools) of dry tomato skins obtained by the OPC-TD method will prove useful during thermal processing and storage.

V. CONCLUSION

In conclusion, the OPC method was applied here to determine thermal diffusivity of the tomatoes characterized by three different stages of maturity. Due to the difficulties experienced when investigating skins of whole fruit the geometry of which was not flat, it was necessary to separate thin skin from a more wet pulp fraction. Careful separation of the skin helped to preserve its original properties. The moisture

levels of all investigated skins were the same. This is an attempt to ensure that the product of thermal diffusivity α and the period of time simulate, as close as possible, a natural trend of maturity. Furthermore, the procedure used here to produce the skin of satisfactory flatness is regarded as an essential step.

During last two decades, the OPC approach was used successfully to obtain thermal diffusivity for a wide range of materials. The outcome of study described in this paper indicates that OPC is at present not the optimal method to unravel each particular feature of complex materials or their entire structures. Nevertheless, the proposed methodology can be used to characterize optical and thermal properties, and in addition to provide the relationship between these properties and microstructures that constitute the materials. This in turn is of particular importance in studies of biological samples such as leaves fruit and vegetables.

Better correlation between thermal diffusivity and the stage of maturity may perhaps be obtained by performing the non-destructive measurements on the intact fruit-preliminary preparations for such experiments are already in progress.

[1]B. A. M. Carciofi, J. Faistel, G. M. F. Aragao, and J. B. Laurindo, J. Food. Eng. **55**, 89 (2002).
[2]Y. Choi and M. R. Okos, Trans. ASAE **26**, 305 (1983).
[3]G. Betta, M. Rinaldi, D. Barbanti, and R. Massini, J. Food. Eng. **91**, 34 (2009).
[4]A. Mandelis and P. Hess, *Progress in Photothermal and Photoacoustic Science and Technology*, Life and Earth Sciences Vol. III (SPIE Optical Engineering, Bellingham, Washington, USA, 1997).
[5]C. L. Cesar, H. Vargas, J. Pelzl, and L. C. M. Miranda, J. Appl. Phys. **55**, 3460 (1984).
[6]L. F. Perondi and L. C. M. Miranda, J. Appl. Phys. **62**, 2955 (1987).
[7]J. Buys, D. Bicanic, J. Bontsema, and H. Vargas, Anal. Instrum. (N. Y.) **20**, 45 (1992).
[8]S. M. Brown, D. Bicanic, and K. van Asselt, J. Food. Eng. **28**, 211 (1996).
[9]M. Yañez-Limón, M. E. Rodríguez, J. J. Alvarado-Gil, O. Zelaya-Angel, F. Sánchez-Sinencio, A. Cruz-Orea, H. Vargas, J. D. C. Figueroa, F. Martínez-Bustos, J. L. Martínez, J. González-Hernández, C. Argüello, and L. C. M. Miranda, Analyst (Cambridge, U.K.) **120**, 1953 (1995).
[10]S. Sánchez-Rocha, M. Vargas-Luna, G. Gutiérrez-Juárez, R. Huerta-Franco, and V. Olalde-Portugal, Int. J. Thermophys. **29**, 2206 (2008).
[11]M. G. da Silva, J. G. Oliveira, A. P. Vitoria, S. F. Corrêa, M. G. Pereira, E. Campostrini, E. Santos, A. Cavalli, and H. Vargas, J. Phys. IV **125**, 877 (2005).
[12]D. T. Dias, J. Mura, M. L. Baesso, A. N. Medina, A. C. Bento, and J. Shen, J. Phys. IV **125**, 383 (2005).
[13]A. Gijsbertsen, D. Bicanic, J. L. W. Gielen, and M. Chirtoc, Infrared Phys. Technol. **45**, 93 (2004).
[14]X. Guo, D. Bicanic, R. Imhof, P. Xiao, and J. Harbinson, Appl. Phys. B: Lasers Opt. **79**, 793 (2004).
[15]M. Hernández, E. Rodriguez, and C. Diaz, J. Agric. Food Chem. **55**, 8604 (2007).
[16]E. Garcia and D. M. Barrett, J. of Food Process. Pres. **30**, 56 (2006).
[17]K. M. Moneruzzam, A. B. M. S. Hossain, W. Sani, and M. Saifuddin, Am. J. Biochem. Biotechnol. **4**, 329 (2008).
[18]F. A. McDonald and G. C. Wetsel, J. Appl. Phys. **49**, 2313 (1978).
[19]P. Charpentier, F. Lepoutre, and L. Bertrand, J. Appl. Phys. **53**, 608 (1982).
[20]G. Rousset, F. Lepoutre, and L. Bertrand, J. Appl. Phys. **54**, 2383 (1983).
[21]K. Hane, T. Kanie, and S. Hattori, Appl. Opt. **27**, 386 (1988).
[22]D. N. Njie, T. R. Rumsey, and R. P. Singh, J. Food. Eng. **37**, 63 (1998).

[23]C. Gordon and S. Thorne, J. Food. Eng. **11**, 133 (1990).

[24]A. Lopes Ramos, E. Palmisano, A. Dombey, J. A. Pimentel, D. Fayes, and D. Gonzalez-Mendizabel, Rev. Esp. Cienc. Technol. Alimentos **33**, 271 (1993).

[25]V. C. Mariani, A. G. B. de Lima, and L. S. C. Coelho, J. Food. Eng. **85**, 569 (2008).

[26]M. F. van Gelder, PhD dissertation, "A thermistor based method for measurement of thermal conductivity and thermal diffusivity of moist food materials at high temperature," Virginia Tech., 1993.

[27]L. Huang and L. S. Liu, J. Food. Eng. **95**, 179 (2009).

[28]T. R. A. Magee and T. Bransburg, J. Food. Eng. **25**, 223 (1995).

[29]H. Bargel and C. Neinhuis, J. Exp. Bot. **56**, 1049 (2005).

[30]V. Hershko, H. D. Rabinowitch, and A. Nussinovitch, Lebensm.-Wiss. Technol. **27**, 386 (1994).